Geochemistry Geophysics Geosystems G3

Article
Volume 13, Number 1
18 January 2012
Q01W09, doi:10.1029/2011GC003808
ISSN: 1525-2027

Published by AGU and the Geochemical Society

A geodynamic model of plumes from the margins of Large Low Shear Velocity Provinces

Bernhard Steinberger

Helmholtz Centre Potsdam, GFZ German Research Centre for Geosciences, D-14473 Potsdam, Germany (bstein@gfz-potsdam.de)

Physics of Geological Processes, University of Oslo, Blindern, N-0316 Oslo, Norway

Trond H. Torsvik

Physics of Geological Processes, University of Oslo, Blindern, N-0316 Oslo, Norway

Center for Geodynamics, Geological Survey of Norway, Leiv Eirikssons vei 39, N-7491 Trondheim, Norway

School of Geosciences, University of the Witwatersrand, Wits 2050, South Africa

[1] We present geodynamic models featuring mantle plumes that are almost exclusively created at the margins of large thermo-chemical piles in the lowermost mantle. The models are based on subduction locations and fluxes inferred from global plate reconstructions and ocean floor paleo-ages. Sinking subducted slabs not only push a heavy chemical layer ahead, such that dome-shaped structures form, but also push the thermal boundary layer (TBL) toward the chemical domes. At the steep edges it is forced upwards and begins to rise — in the lower part of the mantle as sheets, which then split into individual plumes higher in the mantle. The models explain why Large Igneous Provinces – commonly assumed to be caused by plumes forming in the TBL above the core-mantle boundary (CMB)– and kimberlites during the last few hundred Myr erupted mostly above the margins of the African and Pacific Large Low Shear Velocity Provinces (LLSVPs) of the lowermost mantle, which are probably chemically distinct from and heavier than the overlying mantle. Our models support that mantle plumes are more intimately linked to plate tectonics than commonly believed. Not only can plumes cause continental break-up, but conversely subducted plates may trigger plumes at the margins of LLSVPs near the CMB.

Components: 10,700 words, 8 figures.

Keywords: Large Igneous Provinces (LIPs); Large Low Shear Velocity Provinces (LLSVPs); subduction zones.

Index Terms: 8121 Tectonophysics: Dynamics: convection currents, and mantle plumes; 8137 Tectonophysics: Hotspots, large igneous provinces, and flood basalt volcanism; 8170 Tectonophysics: Subduction zone processes (1031, 3060, 3613, 8413).

Received 19 July 2011; **Revised** 29 November 2011; **Accepted** 30 November 2011; **Published** 18 January 2012.

Steinberger, B., and T. H. Torsvik (2012), A geodynamic model of plumes from the margins of Large Low Shear Velocity Provinces, *Geochem. Geophys. Geosyst.*, *13*, Q01W09, doi:10.1029/2011GC003808.

Theme: Plate Reconstructions, Mantle Convection, and Tomography Models: A Complementary Vision of Earth's Interior
Guest: C. Gaina, L. Liu, K. Sigloch, and B. Steinberger

1. Introduction

[2] Plate tectonic theory provides a framework for understanding volcanism at plate boundaries, but fails to explain the distribution of intraplate volcanism — so-called hot spots — and episodes of intense volcanism in the form of Large Igneous Provinces (LIPs) in space and time. Commonly, a deep origin from the base of the mantle [*Wilson*, 1963; *Morgan*, 1971, 1972; *Richards et al.*, 1989] is assumed, but the opposite view of a shallow origin [*Anderson*, 1981] also exists. In the case of a deep origin, we can more specifically ask which features of the lowermost mantle influence where and when "mantle plumes" are generated. Evidently a model that can explain the relation of LIPs and hot spots to features of the deep mantle yields further support to a plume origin in the deep mantle. Reconstructions of the eruption sites of LIPs [*Torsvik et al.*, 2006] and kimberlites [*Torsvik et al.*, 2010] in a mantle reference frame [*Torsvik et al.*, 2008; *Steinberger and Torsvik*, 2008] as well as present-day plume locations [*Thorne et al.*, 2004] indicate that most of these plumes form at the edges of the Large Low Shear Velocity Provinces (LLSVPs) of the lowermost mantle. In this paper, we ask what is necessary to create such a pattern of plume distribution. We find that it is sufficient to include the following ingredients:

[3] (i) a thermal boundary layer (TBL), that is caused by heat diffusing in radial direction from the core into the mantle, and in which viscosity is sufficiently reduced

[4] (ii) subducted lithospheric slabs sinking to the bottom of the mantle

[5] (iii) a discontinuous chemically dense layer at the base of the mantle.

[6] There is evidence for the existence of all three of these features or processes, and we will present here a geodynamic model of plumes rising from LLSVP margins, which is based on the subduction history in recent plate tectonic and paleogeographic reconstructions.

[7] Notably, these three components had been included in previous models [e.g., *McNamara and Zhong*, 2005] but these did not focus on the pattern of plumes relative to the pile margins.

[8] Estimates of heat flux from the core into the mantle are widely discrepant [*Lay et al.*, 2008], because of large uncertainties in both the temperature contrast across the TBL at the base of the mantle and a wide range of estimates (varying by a factor ~5) for the thermal conductivity of lower mantle materials [*de Koker*, 2010; *Goncharov et al.*, 2009, 2010; *Hofmeister*, 2008; *Stackhouse et al.*, 2010], but the existence of a TBL is expected to lead to the formation of deep mantle plumes [*Loper and Stacey*, 1983]. Slabs appear to eventually sink to the base of the mantle [*Grand et al.*, 1997; *van der Meer et al.*, 2010]. *Nataf* [1991] suggests that "the presence of cold slabs is vital for the formation of hotspots," and the development of plumes on the edge of slabs has been modeled by *Tan et al.* [2002].

[9] Two large regions of low seismic wave speed beneath the Pacific and Africa could already be seen in early tomography models [*Dziewonski*, 1984] and have remained a consistent feature since then. De-correlation of p- and s-wave anomalies in the lowermost mantle [*Masters et al.*, 2000], explicit density models [*Ishii and Tromp*, 2004; *Trampert et al.*, 2004], the sharp and steeply dipping edges of LLSVPs [*Ni et al.*, 2002; *Wang and Wen*, 2004] as well as their long-term stability, inferred from the fact that even LIPs and kimberlites of 300 Ma and older are mostly reconstructed to their present-day margins [*Torsvik et al.*, 2006] support the notion that they are chemically distinct from and heavier than the overlying mantle. Partial melting may occur in this thermo-chemical boundary layer [*Lay et al.*, 2004]. Previous numerical models showed that with the appropriate chemical density contrast, a hot but chemically heavier layer is formed into piles [*Gurnis*, 1986; *Tackley*, 1998; *Nakagawa and Tackley*, 2005]. However, in these models, plumes do not preferentially form above the pile margins – rather above their centers. Due to the Earth's subduction history, those piles or domes can obtain shapes similar to the observed LLSVPs [*McNamara and Zhong*, 2005]. *Bull et al.* [2009] have analyzed what these piles would look like under a tomographic inversion – which is important, since the modeling results are compared to tomographic images. With a higher bulk modulus inside the chemical piles, as strongly suggested by seismologic inversions, resulting in a depth-dependent density contrast to the surrounding mantle, the piles can have steep margins [*Tan and Gurnis*, 2005]. *Jellinek and Manga* [2002, 2004] find that plumes often rise above peaks in the dense chemical layer, however, in their models, these peaks do not primarily occur along the margins. It can hence be expected that, if peaks would primarily occur along steep margins, plumes should also primarily rise from these margins [*Garnero et al.*, 2007; *Garnero and McNamara*, 2008]. *Tan et al.* [2011] find that

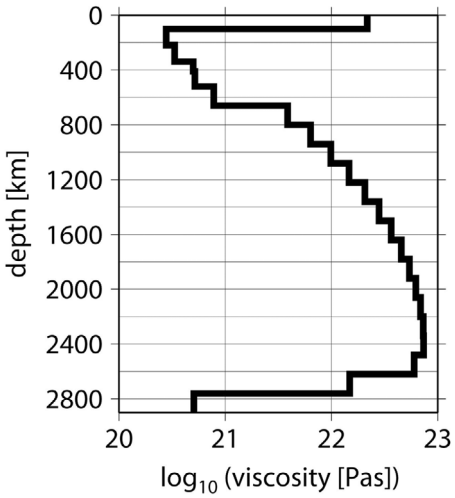

Figure 1. Radial mantle viscosity structure used [*Steinberger and Calderwood*, 2006].

with reasonable values of bulk modulus and density anomalies, the anomalous material forms dome-like structures with steep edges, which can survive for billions of years before being entrained. They find that more plumes occur near the edges, rather than on top, of the chemical domes. Moreover, they find that plumes near the edges of domes have higher temperatures than those atop the domes.

[10] Taking the above ingredients (i)–(iii), and the ideas put forward in the above-cited papers, a conceptual model for the formation of plumes at LLSVP margins is that (a) slabs sinking to the CMB push the TBL to the side, and (b) when the hot material pushed ahead of slabs reaches the steep margins of the heavier LLSVPs, it is forced upward. In vertical direction, the hot and buoyant layer is thus thicker at the margins. In a form of "edge-driven convection," thermal instabilities are created and plumes are formed. We construct here, by successively introducing ingredients (i)–(iii), a numerical geodynamic model, based on spherical harmonic expansion, that confirms our conceptual model.

2. Methods

[11] To compute mantle density and flow over time, we solve equations corresponding to conservation of mass, momentum and energy. Furthermore, we consider the advection of compositional density anomalies. The mantle is modeled as a viscous spherical shell of 6371 km outer radius and 3471 km inner radius, with radially varying viscosity and free-slip upper and lower boundaries (see below for details). The radial viscosity structure, which was derived by *Steinberger and Calderwood* [2006] from mineral physics and surface observations, is shown in Figure 1. Essentially, the shape of the viscosity profile in the different layers of the mantle is derived from radial pressure and temperature profiles, and a realistic model of the dependence of viscosity on these. The absolute value of viscosity in these layers is then adjusted such that a good fit to the geoid, a realistic radial heat flux profile, and a "Haskell average" consistent with postglacial rebound observations is obtained. Lateral viscosity variations are not considered. The mantle is treated as either incompressible, or as compressible and using the PREM [*Dziewonski and Anderson*, 1981] lower mantle parameters for the reference density profile ρ(r).

[12] Equations for conservation of mass and momentum are

$$(\rho u_i)_{,i} = 0 \tag{1}$$

$$-\delta p_{,i} + \left(\eta\left(u_{i,j} + u_{j,i} - \tfrac{2}{3}u_{k,k}\delta_{ij}\right)\right)_{,i} - \delta\rho g\delta_{ir} - \rho\delta g_i = 0 \tag{2}$$

where ρ is (reference) density, u is velocity, δp is pressure anomaly, η is viscosity, δ_{ij} is the Kronecker delta tensor, $\delta\rho$ is the density anomaly, g is the (reference) gravitational acceleration, δg is gravity anomaly, subscript i symbolizes spatial component i and subscript ,i derivative in direction of i. That means we consider the density anomalies only for the buoyancy force term (last term) in the momentum equation, not in the conservation of mass equation. The momentum equation contains a pressure gradient term, a viscous term and a buoyancy term. The viscous term is for a Newtonian viscous rheology, the buoyancy term for vertical gravity (symbolized by δ_{ir}). Reference gravity g is assumed constant at 10 m/s^2, however the effect of gravity anomalies on reference density is also considered. Other force terms – including inertial, Coriolis and centrifugal – are not considered.

[13] Mass and momentum equations are solved with a spherical harmonic approach [*Hager and O'Connell*, 1979, 1981], modified to account for compressibility (following *Panasyuk et al.* [1996]) to degree and order l_{max} = 127 for models shown, yielding the instantaneous relation between density and flow. A test case with l_{max} = 255 ascertains that results do not substantially depend on the maximum degree of expansion. In the model cases without chemical anomalies, density is evaluated on an equidistant radial grid with 57 layers (depths 50 km

to 2850 km). In cases with chemical anomalies, we use 78 layers with a narrower spacing in the lower mantle: 20 km spacing from 2400 to 2880 km depth, 30 km spacing from 2100 to 2400 km, 40 km spacing from 1700 to 2100 km, 50 km spacing above. Velocity is additionally evaluated at the surface and the core-mantle-boundary (CMB).

[14] For each spherical harmonic degree and order, the equations governing instantaneous flow reduce to a system of ordinary differential equations as a function of radius. Starting from initial values corresponding to the bottom boundary condition, three independent solutions of the homogeneous equation – corresponding to the three quantities tangential velocity, radial stress and gravity (potential) that are not constrained to be zero at the CMB – and one solution of the inhomogeneous equation are propagated to the top boundary. The general solution is the sum of the inhomogeneous solution and a linear combination of the homogeneous solutions, and the three free parameters of the general solution are determined by matching the top boundary conditions. In practice, we find that for spherical harmonic degrees higher than about $l = 50$, the four solutions propagated from the CMB to the surface become so large that, even with double precision, we cannot determine a linear combination matching the top boundary conditions (zero tangential stress and zero radial velocity; all gravity sources inside). This problem could be properly addressed with even higher precision arithmetic. Here we circumvented this problem by using a no-slip boundary at depth $50/l \cdot 2900$ km for $l > 50$, in which case the top boundary condition can be matched with sufficient accuracy. In the lowermost mantle, the solution is hence only expanded up until degree 50, corresponding to a half-wavelength of 3.6 degrees (in the lowermost mantle about 200 km). We expect that the overall solution is affected by this modification in only a minor way, except that convection in the region of low viscosity in the lowermost mantle is less well resolved: High viscosity in the overlying lower mantle and the neglect of lateral viscosity variations cause that most of convective power there are at longer wavelengths, hence we do not expect that a higher resolution would affect the result there by much. The other region where smaller-scale convection should be important is the asthenosphere. However, this small-scale flow does not extend much into the lower mantle and is hence not much affected by which lower boundary condition is chosen.

[15] We do not explicitly consider temperature anomalies δT, but instead advect absolute thermal density anomalies $\delta\rho_{th} = \delta T\alpha\rho$, i.e., thermal expansivity α is implied to vary with radius proportional to $1/\rho$ (r). Instead of solving the conservation of energy equation we hence solve

$$\delta\rho_{th,t} + u_i\delta\rho_{th,i} = \kappa\delta\rho_{th,rr} + \alpha H/c_p + S \quad (3)$$

whereby subscript ,t indicates time derivative, κ is thermal diffusivity, c_p is the heat capacity, H is the heat production rate and S is the prescribed plate buoyancy flux, which does not have a corresponding term in the energy equation but is added here to allow for the prescribed input of slabs at subduction zones, as explained below. The left-hand side corresponds to advection, the first two terms on the right hand side to thermal diffusion in radial (r) direction and heat production. Diffusion in horizontal direction, viscous dissipation and the difference between adiabatic heating and cooling are not considered. The equation for advection of compositional heterogeneities $\delta\rho_c$ is

$$\delta\rho_{c,t} + u_i\delta\rho_{c,i} = 0 \quad (4)$$

i.e., it is equivalent to (3) reduced to the advection term.

[16] Thermal diffusion causes that a TBL can form at the base of the mantle from which plumes can rise. We use here a diffusivity of $0.95 \cdot 10^{-6}$ m^2/s. For c_p = 1250 J/kg/K [*Schubert et al.*, 2001] and ρ = 5500 kg/m^3 this corresponds to a thermal conductivity of 6.5 W/m/K, somewhat above the lower end of the range of thermal conductivity estimates for the lowermost mantle, which vary by a factor of ~5 [e.g., *de Koker*, 2010; *Goncharov et al.*, 2009, 2010; *Hofmeister*, 2008; *Stackhouse et al.*, 2010]. We use an isothermal boundary condition and assign a relative density contrast of −1.2% or −0.7% (with a thermal expansivity of 10^{-5}/K corresponding to 1200 K or 700 K) to the CMB. In cases where we already explicitly add density anomalies corresponding to subduction, it would be inappropriate to additionally include a top TBL, therefore we use a top boundary condition corresponding to an insulating surface. In the case without subduction, an isothermal boundary condition TBL with a thermal density contrast of 0.5% is assigned to the surface. We use PREM lower mantle parameters to convert from relative to absolute density contrast.

[17] Thermal Rayleigh number is defined as $Ra_{th} = \Delta\rho_{th}gD^3/(\eta\kappa)$, whereby $\Delta\rho_{th}$ is the (non-adiabatic) thermal density contrast across the mantle and D is its thickness 2900 km. If we use $\eta = 10^{22}$ Pas, which, according to Figure 1, appears appropriate for a (logarithmic) depth average, and other values according to what is given above, we obtain a

Rayleigh number $1.0–2.1 \cdot 10^6$. This rather low value (compared to what is given in many other modeling papers) is mainly due to the high viscosity value used and because we use mantle thickness rather than Earth radius to define Rayleigh number.

[18] For the internal heating term $\alpha H/c_p$, we use $\rho(r) \cdot 7.57 \cdot 10^{-7}$/Myr, corresponding to a total heat flux of about 6 TW from internal heating. This value only affects mean temperature and hence conductive heat transport in the TBLs, but should not affect flow structure and lateral density heterogeneities, which we are concerned about in this paper. Since equation (3) does not explicitly contain temperature, we do not need to separately give values for α and c_p; they are only needed when we convert our results a posteriori to temperatures and heat fluxes.

[19] Time integration of equations (3) and (4) is performed on a grid using a 4th order Runge-Kutta scheme [*Press et al.*, 1986]. For the advection term, we use an upwind differencing scheme [*Press et al.*, 1986] to overcome numerical instabilities in the advection. We use a time integration step such that the advection per step is at most 12.5 km, less than the smallest radial grid spacing (20 km). In this way, we find no instabilities developing during the advection of thermal and chemical anomalies. However, our results are affected by numerical diffusion, even in the case of chemical anomalies, where equation (4) contains no explicit diffusion term.

[20] Solving the equations for the conservation of energy and the advection of compositional density anomalies allows us to compute the evolution of thermal and chemical density heterogeneities forward in time. Since mass and momentum equations are solved in the spectral domain but the energy equation on a grid, it is necessary to transform densities and flow between the two domains at each time step. This is facilitated by using a grid of $l_{max}+1$ "Gaussian" latitudes – meaning that the cosines of colatitude equal the integration points of Gaussian quadrature over the interval [−1,1] [see, e.g., *Press et al.*, 1986] – and $2l_{max} + 2$ equidistant longitudes.

[21] The energy equation is modified such that at each time step thermal density anomalies are added to account for subduction. The subduction model has been described by *Steinberger and Torsvik* [2010]: Subduction zone locations are obtained from global plate reconstruction back to 300 Ma, interpolated in 2 Myr intervals. Back to 140 Ma we also use information on convergence rate and plate thickness (inferred from the age of the subducted lithosphere) to compute the amount of subducted material per time and length of subduction zone. Before 140 Ma, no reliable information is available for this, and we hence use a constant value, similar to the average value obtained post-140 Ma. Anomalous slab masses are then laterally distributed onto the Gaussian grid of 128 × 256 points. For each subduction zone element, the slab mass anomaly is distributed onto the four surrounding grid points such that the center of mass remains. After spherical harmonic expansion a cosine taper in the degree range 64–127 is applied to avoid "ringing." Subducted slabs are distributed onto 7 radial layers at 150–450 km depth, according to a Gaussian bell shape, i.e., with relative magnitudes 0.037, 0.125, 0.213, 0.25, 0.213, 0.125 and 0.037. Total buoyancy is reduced by 21%, compared to the amount that would be inferred from the ocean floor age-depth relation. Reduced buoyancy may result from subduction of the crustal layer and depleted mantle layer, however we do not aim here at implementing this effect properly. In this way, the prescribed plate buoyancy flux S in equation (3) is obtained. The slab density anomalies are added every 2 Myr. Since they are radially distributed, this time spacing is sufficient to obtain a steadily sinking slab flow. Effects of phase boundaries are disregarded, and slabs sink continuously to the lower mantle. Compared to *Steinberger and Torsvik* [2010] subduction locations are shifted in longitude [*van der Meer et al.*, 2010]. With this shift, modeled thermochemical domes match the observed LLSVPs better in longitude.

[22] Models are initiated at 300 Ma and run until the present. For the initial thermal density model, we use small random fluctuations on the grid points between −0.1% and 0.1% relative density anomaly. In model cases with chemical density contrasts, a compositional density difference of 2.3% is assigned to the bottom three layers, i.e., the bottom 70 km of the mantle. With this thickness, the compositionally distinct basal layer has a volume of about $10.8 \cdot 10^9$ km^3, about 1.2% of the total volume of mantle plus crust, corresponding to the range of estimates $8.8–14.2 \cdot 10^9$ km^3 for the combined volume of the LLSVPs, as given by *Burke et al.* [2008], and slightly less than the estimate 2.0 ± 0.4% given by *Hernlund and Houser* [2008]. In combination with the thermal anomaly −1.2%, which is used at the CMB in this case, the total density anomaly is still at least +1.1%. The chemical density difference 2.3% is similar to what has previously found to be appropriate for the chemical layer to be formed into piles: *Nakagawa and Tackley* [2005] find this behavior with a chemical buoyancy

1.8%, whereas for a larger buoyancy 3.6% the chemical layer remains continuous at the CMB. Similarly, *Tan et al.* [2011] find chemical domes for a chemical density contrast 1.5–2%.

[23] We use two approaches to avoid numerical diffusion and entrainment of the chemical layer. In the first approach, the compositional anomaly is "pushed" to the bottom of the model at each time step: For each lateral grid point location the chemical anomaly is numerically integrated in vertical direction. Then the initial anomaly 2.3% is assigned from the CMB to a depth such that the product of layer thickness and 2.3% is equal to the integral. In the second approach, we model the compositional anomaly through 5,000,000 tracer particles that are initially randomly distributed in the bottom 70 km of the mantle, and with a weight such that the average density anomaly above the CMB is again 2.3%. These are advected in the flow field using a 4th order Runge-Kutta scheme [*Press et al.*, 1986]. In order to keep the chemical anomalies near the base of the mantle, the "weight" of the tracer particles increases with height above the CMB; we assign a weight at radius r proportional to $1 + 10\cdot(r - r_1)/r$ whereby r_1 is the radius of the lowest layer at 2880 km depth.

[24] We note that in the Earth mantle, thermal expansivity may decrease with depth even more strongly than $\sim 1/\rho(r)$ [e.g., *Schubert et al.*, 2001]. This effect would cause thermal density anomalies to become smaller with depth in the mantle. On the other hand, hot upwellings in the mantle cool off more during adiabatic decompression than cold downwellings heat up during adiabatic compression. This effect would cause thermal density anomalies to become larger with depth in the mantle [*Albers and Christensen*, 1996]. Hence the two effects should partly compensate each other and we expect that, given uncertainties, advecting absolute density anomalies is a reasonable approximation.

3. Results

[25] First we introduce a TBL at the CMB. If our model neither contains chemical anomalies nor explicitly prescribed subduction, eventually eleven rather stable plumes form around the globe (Figure 2). To assess their stability, we run this model case for 600 Myr. We find the pattern not strongly changing; plumes are continuously active, but they do slightly move, and occasionally merge, such that the number of plumes at the end of the model run is somewhat less. In this case (without explicitly introducing subduction) we also include a top TBL with a thermal density contrast of 0.5% at the surface. This is less than what would correspond to a realistic temperature contrast across the top TBL, however, this rather small value was chosen such that the bottom TBL destabilizes before the top, in order to study the pattern of upwellings that – in contrast to the models shown later–develops without being triggered by subduction. It may also correspond to the case of a rather rigid lithosphere where only the bottom part destabilizes, such as may be the case for Venus, for most times during its history. Plumes in this model are rather massive; the plume shown in the cross section has a diameter of >1000 km and an anomalous mass flux of about 10^5 kg/s in the mid-mantle, much larger than observation-based estimates [*Sleep*, 1990; *Davies*, 1988]. The diameter is so large because it includes the "thermal halo," and we do not consider temperature-dependence of viscosity. For the case that viscosity inside the conduit is not much smaller than outside, *Steinberger and Antretter* [2006] estimate based on a formula given by *Schubert et al.* [2001] ~500–600 km diameter in the lower half of the mantle for a plume with $4\cdot10^3$ kg/s anomalous mass flux [see *Steinberger and Antretter*, 2006, Figure 6] and a diameter proportional to the fourth root of anomalous mass flux, corresponding to ~1200 km diameter for the model in Figure 2. Hence the large plume diameters in this model appears to be due to model parameters and not due to insufficient model resolution. For comparison we also show in Figure S1 in the auxiliary material a model case with a constant sub-lithospheric viscosity of 10^{21} Pas.[1] In this case, plumes are much narrower and the total number of plumes is much larger, as expected.

[26] The picture, however, changes considerably if we insert subducted slabs as inferred from paleogeographic reconstructions (Figure 3). Then the slabs sinking toward the CMB push the TBL to the side and create upwellings [*Tan et al.*, 2002] (Figure 4). These upwellings form a ring in the Pacific hemisphere. In the African hemisphere they do not form a complete ring; rather a line stretching from Western Europe to the Southern Atlantic and on to the Southern Indian Ocean, plus a separated upwelling further north in the Indian Ocean. This already approximately corresponds to the Plume/LIP pattern, but would correspond to rings of slow seismic velocity in map views of lowermost mantle

[1] Auxiliary materials are available in the HTML. doi:10.1029/2011GC003808.

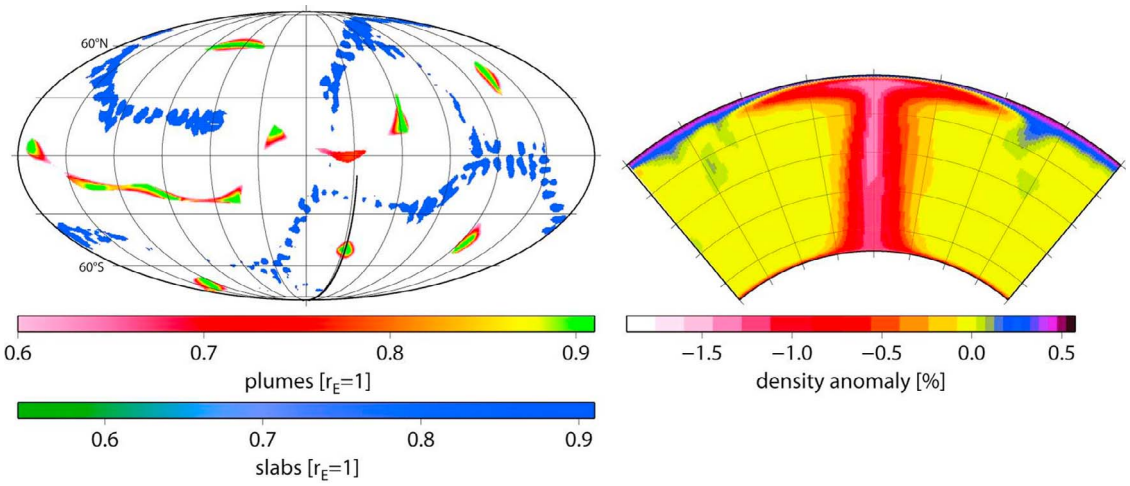

Figure 2. Model results for the case without subduction and without chemical anomalies; CMB thermal density contrast −1.2%; incompressible flow computation. (left) Map view with "plumes" plotted whenever at a depth indicated by the color scale negative thermal density anomalies exceed −0.7%, and "slabs" when positive thermal anomalies exceed +0.1%. (right) Cross section through one of the plumes. Structure is shown 220 Myr after model initiation.

tomography, and the rings getting smaller and smaller with time.

[27] We hence introduce a chemical layer of 2.3% density excess that is initially 70 km thick and homogeneous at the base of the mantle. This chemical layer is formed into "domes" (Figure 5) by the flow driven by subducted slabs. Upwellings now form at the edges of these domes, as in the conceptual model, and are more plume-like, less sheet-like. They only start forming after the first slabs have reached the CMB, i.e., their development is clearly forced by the slabs. The cross-sections in Figure 5 show that the domes can become rather high – up to about 1000 km – at their edges, much more than the typical CMB TBL thickness. Plumes becoming anchored at these topographic highs is hence consistent with the criterion given by *Jellinek and Manga* [2004], who find that the topography has to be at least half the TBL thickness in order for a plume to become anchored. The domes being heavier than surrounding mantle and hence having a tendency to spread out counteracts the rings getting smaller, and with the domes also being hot, the thermal anomalies better resemble tomography (Figure 6). Plumes form preferentially at "corners," and locations of model plumes partly resemble those of actual plumes – Hawaii at a northern corner of the Pacific LLSVP, Iceland at the northwestern corner of the African LLSVP, Kerguelen at its southeastern corner. Plume conduits tend to get tilted – with bases moving toward the centers and tops remaining closer to the margins of domes, like in a previous simpler model [*Steinberger and O'Connell*, 1998]. Such tilted plumes match better with tomography than straight ones [*Boschi et al.*, 2007]. Occasionally subduction moving toward the Pacific dome erodes off parts of it, and plumes become separated or form above a separated part. One of those split-off plumes might correspond to the Columbia River Basalts/Yellowstone plume, another one to a smaller Low Shear Velocity Province and possibly plume beneath Russia and Kazakhstan.

[28] Comparison of the "LIP" locations where plumes initially reach the surface and the present-day plume locations shows that, for the models in Figures 6 and 7 (except Figure 7d) in most cases a LIP can be associated with a plume, i.e., plumes remain active since their initiation up to 140 Myr ago. Comparison also shows that plumes tend to be displaced toward the centers of domes compared to their corresponding LIP, i.e., they tend to migrate slowly toward the centers of large-scale upwellings. Although we do not attempt a quantitative assessment, we observe that displacements are typically 1000–2000 km or less. Given a typical time span of 100 Myr, this corresponds to a speed of motion 1–2 cm/yr or less, in accordance with observations and earlier models of hot spot motion [*Steinberger*, 2000] for most hot spots.

[29] Comparison of compressible and incompressible model cases shows no major differences. In the first case, flow speeds in the lower mantle tend to be somewhat slower, corresponding to compression. Accordingly, plumes tend to form, and reach the surface somewhat later. Therefore, computed

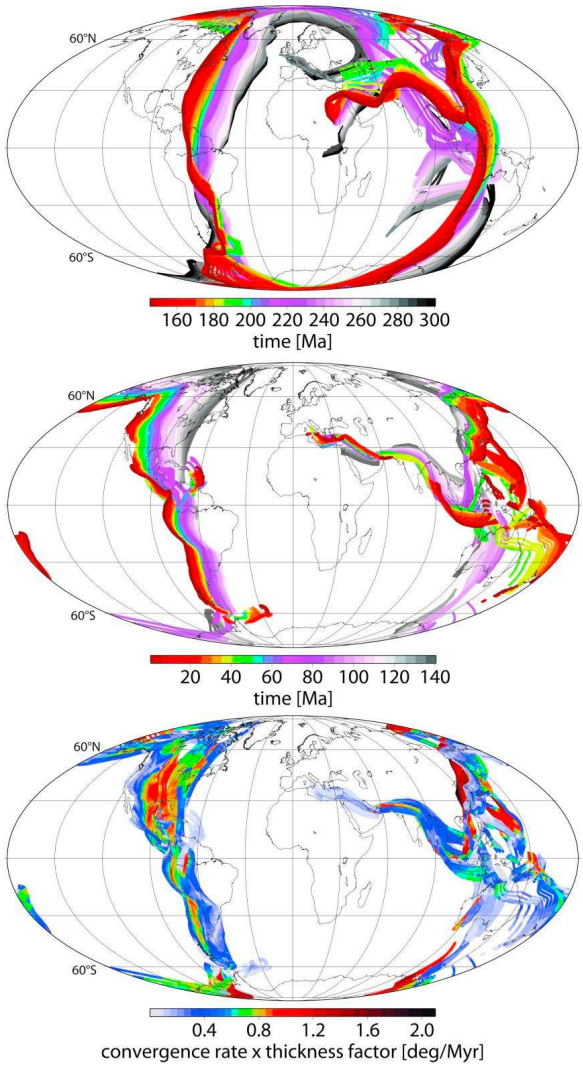

Figure 3. (top) Subduction zone locations 300–140 Ma. (middle) Subduction zone locations 140 Ma – present. (bottom) Amounts of subduction, proportional to anomalous mass flux per subduction zone length, since 140 Ma. For the thickness factor, the square root of age of subducted lithosphere divided by 80 Myr is used for ages < 80 Myr, and 1 is used for ages > 80 Myr. Compared to our previous model [*Steinberger and Torsvik*, 2010] slabs are shifted in longitude [*van der Meer et al.*, 2010].

present-day hot spots tend to be located, and displaced relative to their corresponding LIPs slightly less toward the centers of the domes (compare Figures 6 (top) and 7a). To test the effect of thermal expansivity versus depth on our model results, we have also computed a model where thermal density anomalies decrease with depth corresponding to a decrease of thermal expansivity by about a factor five from top to bottom of the mantle. Again, we find no major difference in results, but upwellings tend to remain slightly more sheet-like along margins of domes and less plume-like.

[30] To assess the effect of the model initiation, we also consider a case where we initiate the model without subduction at 480 Ma, and initiate subduction at 300 Ma, such that a CMB TBL has already developed when subduction starts. In this case, results remain similar, except that plumes start developing earlier. As a result, computed present-day hot spot locations are again further toward the centers of domes. Second, we re-run the model by taking the computed present-day state as initial condition at 300 Myr. We then find a larger number of plumes than LIPs (Figure 7d), representing that plumes from the previous model cycle have still survived, and thus can be very long-lived in our model, with life spans exceeding 300 Myr. In this case, the locations of domes are remarkably stable; plumes tend to be more frequent over their centers – again an effect of their tendency of migrating (rather than forming) there: the locations where plumes initially form still tend to concentrate above the dome margins. Further, we initiate a model without subduction even earlier, at 750 Ma, such that plumes have fully developed at the time we insert the first slab (similar to Figure 2, but with chemical layer): In this case, pre-existing plumes are mainly being moved around, rather than newly created due to the sinking of slabs, i.e., the model case with pre-existing plumes is less successful in recreating the pattern of plumes originating at the margin of piles.

[31] Apart from this case, the basic results of plumes forming at margins of domes are obtained regardless of whether one of the "anti-diffusion" measures described in section 2 is applied or not. The difference is merely that, without these, the modeled domes shrink substantially over the model run (300 Myr) which is probably unrealistic, given they appear to be stable over this time period [*Torsvik et al.*, 2006]. We hence prefer to show the results, where one of the two approaches to counteract diffusion has been taken. In the first one (as in Figures 5 and 6), we "push" the chemical layer to the bottom of the model after each advection time step. This counteracts entrainment of the chemical layer, regardless whether it is a realistic model feature or due to numerical diffusion. In order to only counteract the latter, we model in our second approach the chemical layer through tracer particles. However, we find that then the chemical layer gets mixed with the overlying mantle and thus diluted. Therefore, even though the chemical density anomaly initially exceeds the maximum

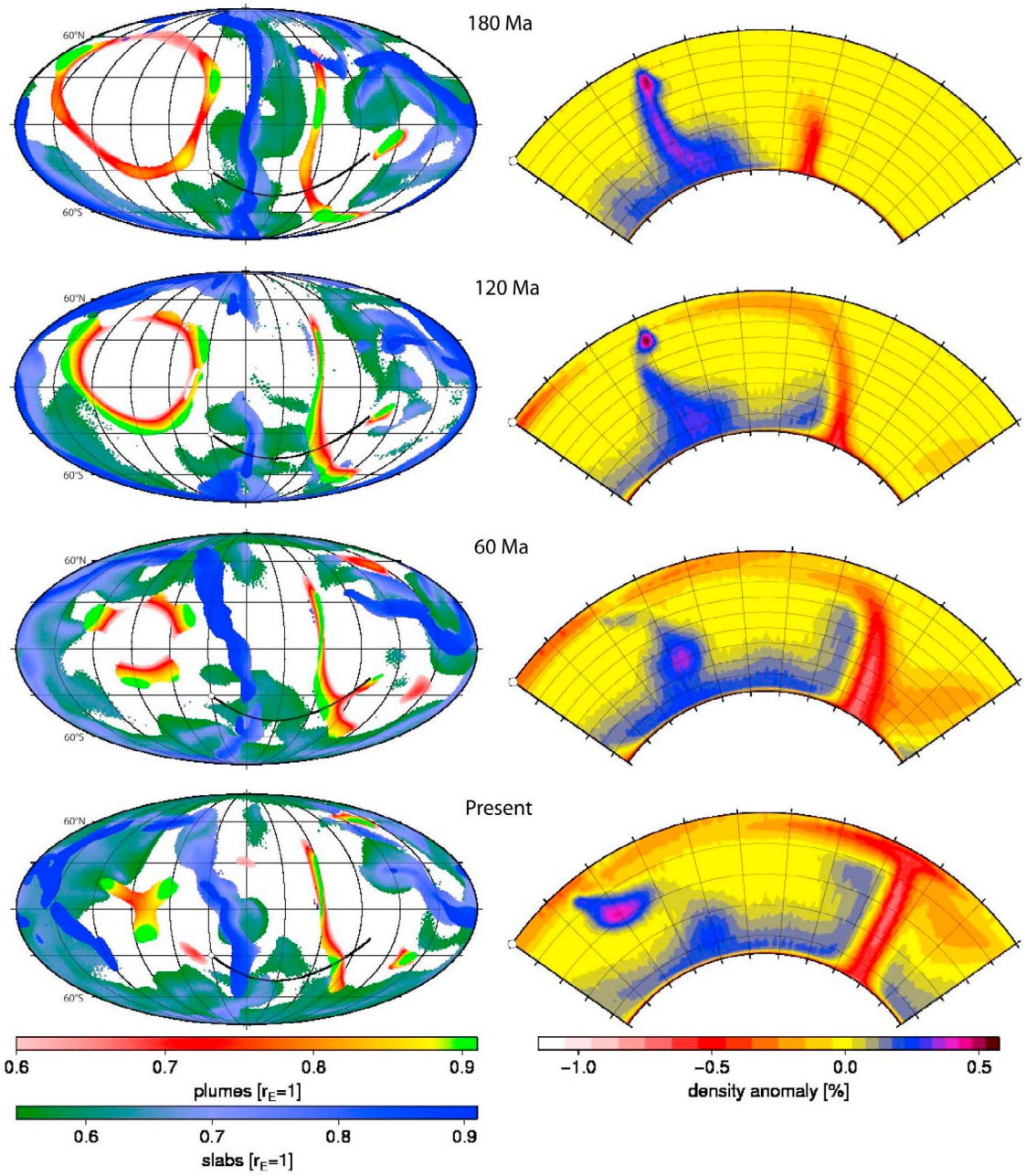

Figure 4. Model results without chemical anomalies. Distribution of thermal anomalies (slabs and plumes) in the mantle at different times. CMB thermal density contrast −0.7%; incompressible flow computation. (left) Map view (centered on 60°W) with "slabs" plotted whenever at a depth indicated by the color scale positive thermal density anomalies exceed +0.2%, and "plumes" when negative thermal anomalies exceed −0.25%. (right) Cross section along the black line in the maps through the subduction zone under South America and the resulting upwelling under the South Atlantic for the same times.

thermal density anomaly, it becomes gradually less. Therefore, if the mass of a tracer particles does not depend on depth, the chemical layer does not remain stably at the base of the mantle over the 300 Myr model run. To counteract this, and keep the chemical layer near the base of the mantle we let tracer particles become heavier higher up in the mantle, similar to what has been proposed by *Tan and Gurnis* [2005]. Then we again obtain similar results for both compressible and incompressible flow computations (Figure 7).

[32] Figure 8 shows the total heat flux through the mantle in our models as a function of time, indi-

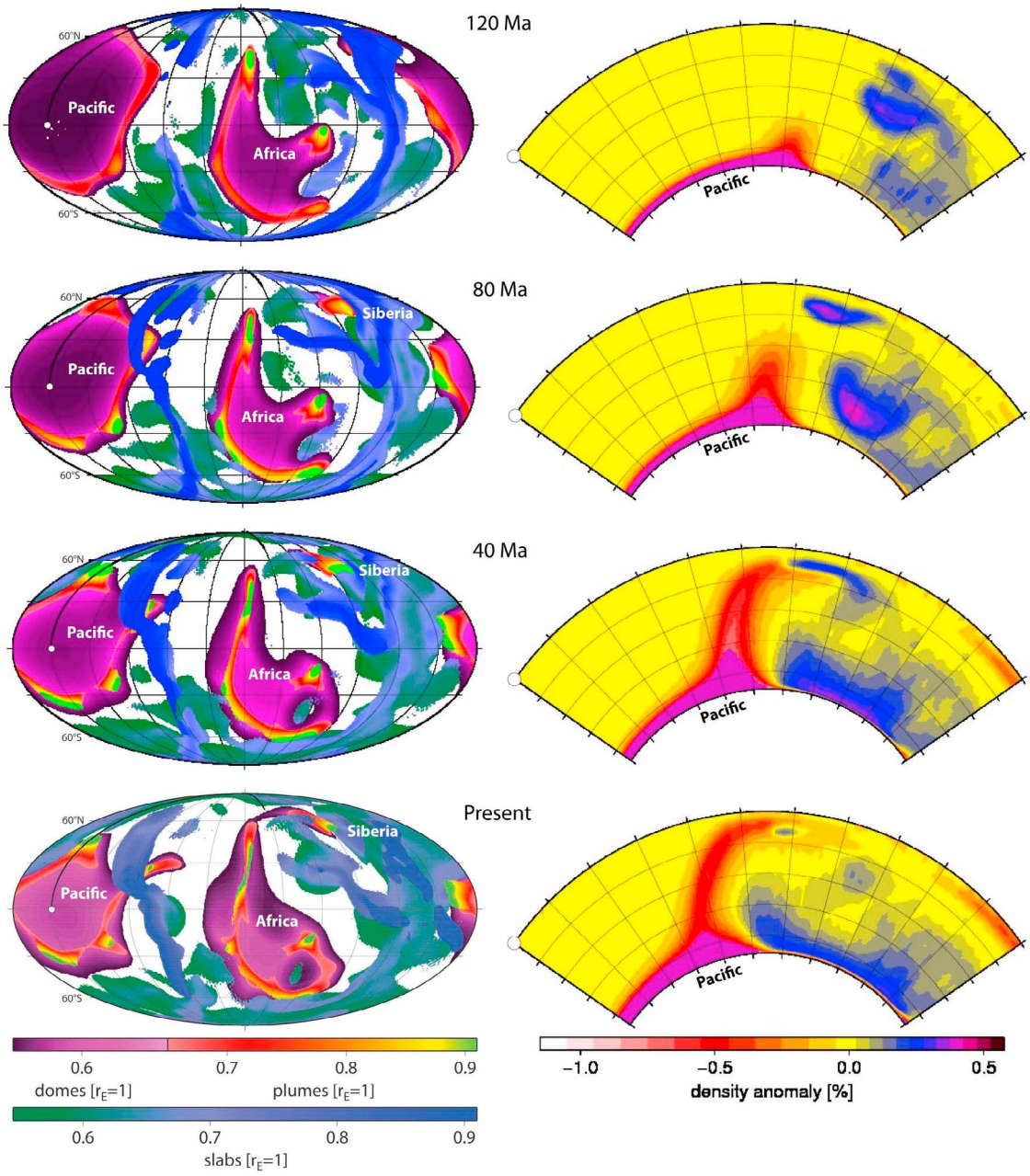

Figure 5. Distribution of thermal anomalies (slabs and plumes) and chemical anomalies ("domes") in the mantle at different times. CMB thermal density contrast −1.2%; compressible flow computation. (left) Map view (centered on Greenwich) with "slabs" plotted whenever at a depth indicated by the color scale positive thermal density anomalies exceed +0.2%, and "plumes" when negative thermal anomalies exceed −0.25%. "Domes" are plotted when compositional density anomalies exceed 1.15%. (right) Cross sections at 150°W through the modeled "Hawaii plume" for the same times, showing thermal density anomalies and chemical domes (in violet).

cating approximately earth-like values for the present-day mantle heat flux of around 30 TW. Black and red lines (corresponding to the two different methods of modeling chemical anomalies) are nearly identical as long as heat flux is primarily through subducted slabs in the model (until ~150 Ma, except for the "re-start" case). Differences between the red line models (where plumes start rising earlier) and the corresponding black line models, as well as differences between the dotted line ("re-start" case where plumes rise from the beginning of the model run) and dashed line indicate that the

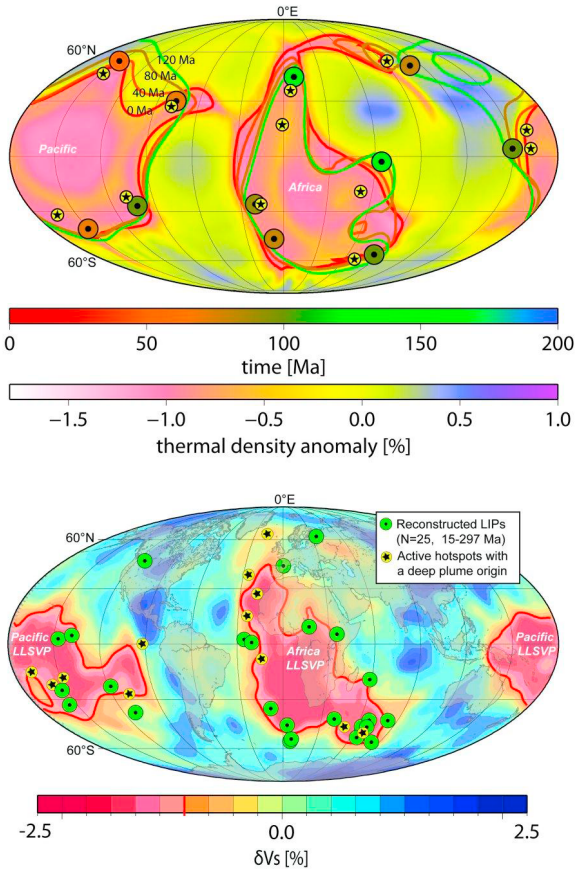

Figure 6. (top) Predicted present-day thermal anomaly at depth 2800 km. Colored lines are the margins of chemical domes at that depth at 120 Ma, 80 Ma, 40 Ma and 0 Ma. Colored circles are the locations where plumes first reach the surface (corresponding to LIPs) with times corresponding to colors. Yellow circles with stars show present-day plume locations. These locations were determined by visual inspection of maps as in Figure 5 (left) in 10 Myr intervals. Sometimes a plume disappears and sometimes it splits into two, therefore not all "LIPs" correspond to exactly one "plume." (bottom) For comparison tomography model SMEAN [*Becker and Boschi*, 2002]. Also shown are reconstructed locations of LIPs as well as present-day hot spot positions [*Torsvik et al.*, 2010].

heat flux accomplished through plumes is about 10 TW in the model. A larger amount of heat flux (time-variable, averaging about 30 TW) is due to subduction of slabs. Heat flux variations – in particular for the "re-start" case, where plumes occur from the beginning – are mostly caused by variations in slab flux over time. Accordingly, anomalous mass flux of individual plumes in this case is about $10–20{\cdot}10^3$ kg/s, much smaller than in the first case without chemical layer, but still much bigger than observation-based estimates. In this case, the formula given by *Steinberger and Antretter* [2006] for the thermal plume diameter gives about 700–800 km. This is again in approximate agreement with the diameter found in our numerical model (Figure 5).

4. Discussion

[33] Our model is initiated at 300 Ma, since we have the most reliable information on subduction locations since then. Previous subduction during formation of Pangaea is less well known. Because of this model limitation, we cannot here address the question whether the two LLSVPs were stable before that, or whether there has been a degree-1 mantle structure during formation of Pangaea [*Zhang et al.*, 2010]. In a complementary approach [*Tan et al.*, 2011] it is found that dome-like and chemically distinct structures at the base of the mantle survive, but are not immobile, for >3Ga, with plumes also often forming near their edges. Because of the much longer time span covered, that approach cannot use a subduction model based on plate reconstructions. We initiate the model with a homogeneous layer, because we believe that is the least "prejudiced" starting condition, not because it is realistic. We use alternative initial conditions, to test their influence on our model. Longer-running models often feature plumes above interiors of domes, but plumes generally don't get generated there; they rather migrate from the margins toward the interiors and in this way can remove heat from the tops of domes. In all our models – so long as they include prescribed subduction zones – plumes get initiated largely or only at the margins of domes, consistent with the observed occurrence of LIPs above LLSVP margins [*Torsvik et al.*, 2006].

[34] Initiating the model with a homogeneous layer causes that the thermo-chemical domes only start forming after subduction is initiated, with their margins initially moving rapidly, whereas reconstructing LIPs to their paleo-position indicates the thermo-chemical domes have not moved much since 200 Ma [*Torsvik et al.*, 2006] or even longer [*Burke et al.*, 2008; *Torsvik et al.*, 2010]. However, the locations of domes in the models become more stable during the times since ~120 Ma when most plumes reach the surface (lines plotted in Figures 6 (top) and 7), or if we initiate the model with pre-existing domes (Figure 7d). Notably, the strongest motion of the margin (in Figures 6 and 7a–7c) tends to occur over the northern Pacific, for which

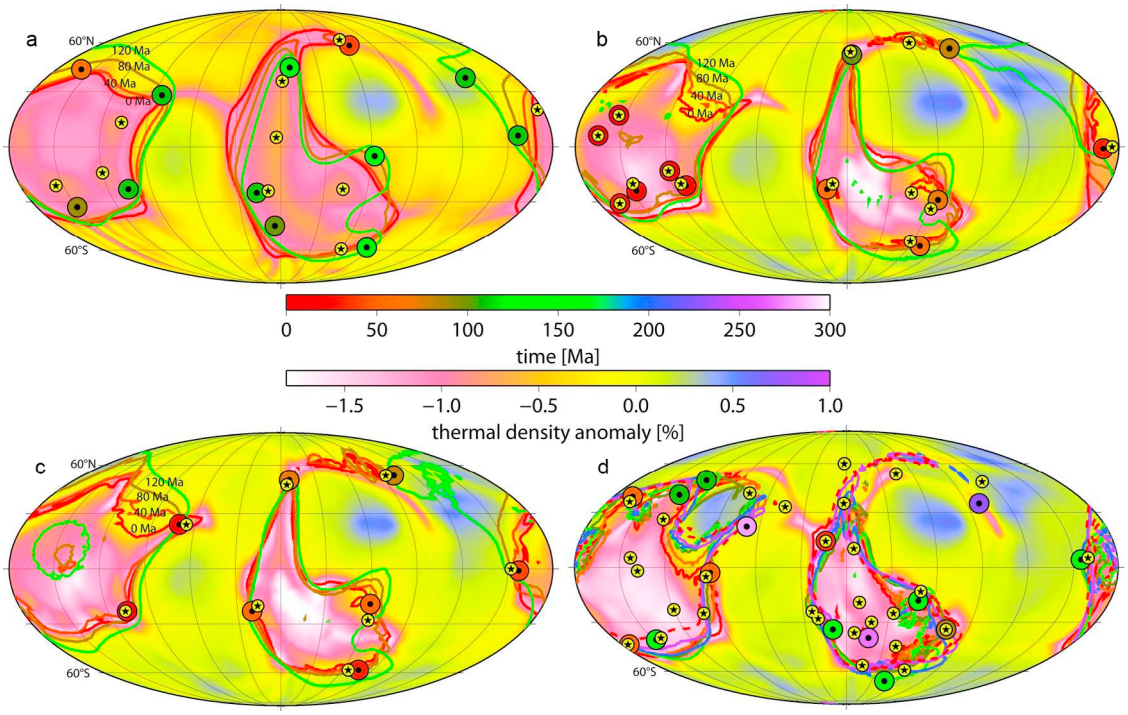

Figure 7. Like Figure 6 (top) but with the following differences: Figures 7a, 7b, and 7d show incompressible flow computation. Figures 7b–7d show compositional variations modeled with tracer particles. Figure 7d shows rerun starting with computed present-day density field as the initial condition at 300 Ma.

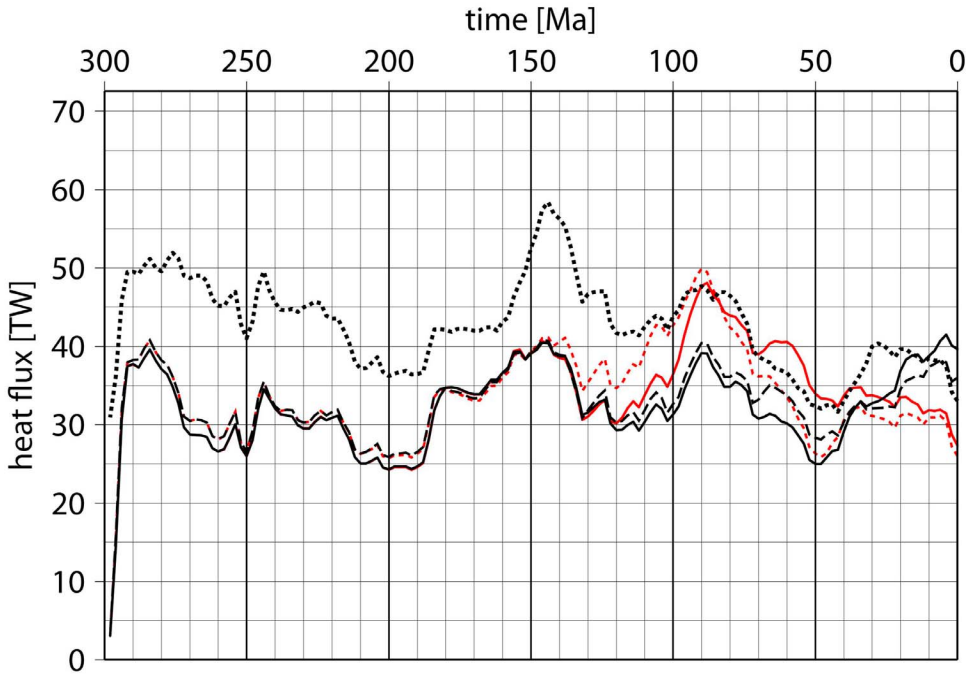

Figure 8. Heat flux versus time. Red continuous: compressible model as in Figures 5 and 6; red dashed: incompressible case as in Figure 7a. Black continuous/dashed: chemical layer modeled as tracer particles (as Figure 7) compressible/incompressible. Black dotted: re-run as in Figure 7d. Anomalous mass flux is computed from flow and density field at depth 450 km and converted to heat flux using a thermal expansivity of $2 \cdot 10^{-5}$/K and a heat capacity of 1250 J/kg/K.

no LIPs are preserved to indicate that it has not moved. In order to properly address the question under which conditions the domes are immobile since 200–300 Ma or longer, it will be necessary to consider plate reconstructions or at least subduction zone locations much further back in time.

[35] Another aspect of the stability of thermo-chemical domes concerns whether their entrainment into plumes is sufficiently low to allow their existence over the larger part of Earth history. Also in this respect, it is not straightforward to maintain them stable through geologic times. Conditions for long-term stability of thermo-chemical piles or "superplumes" were compiled and discussed by *Tackley* [1998] and *Lay et al.* [2004]. An important consideration in this context is to what extent these chemical reservoirs are recharged from the heavy (basaltic) component of subducted slabs, and how effectively this dense component is separated off [*Olson and Kincaid*, 1991; *Tackley*, 2011]. Our measures to counter-act diffusion and entrainment of this thermo-chemical layer into plumes are ad hoc, but the pattern of plumes forming above margins of domes is found regardless of whether or not they are applied (see Figures S2 and S3, for comparison, where no such measures have been taken). What are the real physical mechanisms that allow for long-term LLSVP stability needs to be further addressed in future work.

[36] Our model is simplified in that lateral viscosity variations due to temperature variations are not considered. Although it is not even clear whether higher temperatures lead to a lower viscosity at all [*Korenaga*, 2005], future models should study the effect of temperature-dependent viscosity. We expect that it will mainly lead to thinner, more feeble plume conduits that follow the initially rising plume head, similar to other recent global models [e.g., *Bull et al.*, 2009; *Zhang et al.*, 2009; *Lassak et al.*, 2010], but perhaps not quite as thin, because of the rather high lower mantle viscosity, and correspondingly low effective Rayleigh number in our model. Lower viscosity inside the conduit could lead to faster draining of the TBL, and shorter conduit lifespans [*Davaille and Vatteville*, 2005]. Thinner conduits could also be more easily distorted and disrupted by large-scale flow. The rise of the initial plume head, on the other hand, should be mostly affected by viscosity of the surrounding mantle, hence we expect that the correlation of plume heads with the margins of thermo-chemical piles will not be strongly affected by temperature-dependent viscosity. The plume conduits in our model are long-lived (stable for hundreds of Myr) and if they are more massive than in the real Earth, they should influence large-scale flow more strongly. They thus may affect the sinking of slabs more strongly than in the real Earth. Nevertheless, we find that even in our model, lateral deflection of slabs from vertical sinking is not very strong. Hence we do not expect that including lateral viscosity variations will fundamentally change results.

[37] Another model simplification is that no surface plate motions are imposed, but instead subducted slabs are inserted into the mantle at prescribe locations. This modeling procedure was chosen, since we had a digital model of subduction zone locations in 2 Myr intervals back to 300 Myr [*Steinberger and Torsvik*, 2010], available, but complete plate reconstructions in the required format with closed polygons only in 10 Myr intervals back to 250 Ma. Also, this method gives us better control over the amount of material sinking into the mantle at convergent margins. We have, however, also computed models with imposed surface plate motions and a top thermal boundary layer instead of inserting slabs (shown in Figures S2 and S3). Qualitatively, these models give very similar results; the basal chemical layer is shaped into piles, and plumes rise from their margins. This similarity is not surprising, given that the large-scale mantle flow structure is similar in both cases, with velocities at shallow depth toward subduction zones/convergent margins, and downward flow beneath these. In Figure S3, the absolute plate rotations for all plates in the Pacific basin before 150 Ma (which are unconstrained by hot spot tracks) have been modified by adding 0.4 deg/Ma around an axis parallel to the Earth's spin axis, i.e., an additional eastward component of motion has been added to these plates, relative to Figure S2. This results in more subduction east and less west of the Pacific, hence the distance between the two LLSVPs is larger beneath South America and smaller beneath East Asia. In combination with thinner conduits, resulting from temperature-dependent viscosity, imposing plate motion could lead to less stable plumes and convection. Our previous simple models of plumes in large-scale flow indicate, though, that the effect of prescribed plate motions on the motion of plumes is probably smaller than the effect of internal density heterogeneities [see, e.g., *Steinberger and O'Connell*, 1998, Figures 4 and 5]. Moreover, because – as stated above – the large-scale mantle flow pattern would remain overall rather similar even if we impose plate motions, we do not expect that imposing plate motions would affect plume

stability in a major way. Also, the model of *Tan et al.* [2006] shows that imposing plate motions mainly affects plume conduits in the upper mantle, where the kinematic flow is strongest. Nevertheless, prescribing surface plate motion boundary conditions should be the preferred method in future models, and it will be more straightforward implementing these in short time intervals, using the Gplates software [*Gurnis et al.*, 2012].

[38] Since in our model we impose the locations of subduction as inferred from the history of plate motions, we cannot address the issue as to what extent long-lived LLSVPs and upwellings above them are controls of long-term large-scale mantle structure and hence influence where subduction zones may form [*Dziewonski et al.*, 2010]. Clearly, we expect that processes in the deep Earth influence processes near the surface, and vice versa, but our model by design is restricted to mainly yield the influence of surface processes on the deep Earth.

[39] We have here chosen an initial thickness of the chemical layer 70 km that yields about the right amount of chemically distinct material, as inferred from various observations (see *Burke et al.* [2008] for a compilation of these). However, this amount is uncertain to a large degree. *Jellinek and Manga* [2004] find that plumes become anchored at the peaks of chemical piles or domes if they are at least half as high as the TBL thickness. In our models, they are always higher. A more thorough investigation should test whether in our model the criterion of *Jellinek and Manga* [2004] also holds.

[40] We use a chemical density contrast 2.3%, because in this way, we find the chemical domes acquiring areas similar to the observed LLSVP areas above the CMB. With a larger density contrast, the domes would tend to spread out more and have a larger footprint on the CMB, with a smaller contrast they would be smaller. 2.3% chemical density contrast is also similar to what previous models found appropriate to generate chemical piles [*Nakagawa and Tackley*, 2005; *Tan et al.*, 2011]. In additional model runs, we have also used chemical density contrasts 3.2% and 3%, combined with a thermal density anomaly 2% at the CMB. In all cases, we find a tendency for plumes to occur at the margins of domes. However, some models (e.g., Figure 7d) also feature plumes above their interiors. Typically there are about 4–7 plumes simultaneously reaching the surface in each "domain" (Pacific or African), which is within the range or 3–9 instabilities expected by *Davaille et al.* [2005] for the Indo-Atlantic "box." But some of our models – in particular, "re-start" cases as in Figure 7d – feature a larger number of plumes, as they can remain active for hundreds of Myr in our model.

[41] But in all cases, plumes occur almost only above the geochemical domes, and there are large regions – primarily in the areas where subduction occurred – which are devoid of plumes. This is consistent with previous results that hot plumes form away from downwellings [e.g., *Bunge and Davies*, 2001; *Monnereau and Quere*, 2001], and rather form in regions where the thermal boundary layer is thickest [*Sleep et al.*, 1988]. Our result is also consistent with the laboratory models of *Gonnermann et al.* [2004], from which they inferred that subduction imposes a large-scale structure on mantle flow, thinning the TBL and hence suppressing plume formation over large areas of the CMB. Similarly, the results of *Jellinek et al.* [2003] suggest that large-scale flow focuses plumes toward upwellings in the Central Pacific and Africa, which is also where most plumes occur in our model. In contrast, *Tan et al.* [2002] find besides plumes forming ahead of slabs also occasional "mega-plumes" developing beneath slabs, due to large amounts of heat trapped; *Robin et al.* [2007] observe after subducted material reaches the core-mantle boundary in their model, both "thermals" forming ahead of the advancing cold front and "plumes" forming behind.

[42] We find that a large part (about 30 TW) of heat flux across the mantle in our models is due to subducted slabs and large-scale flow – the initiation of plumes leads to a smaller increase (about 10 TW) in heat flux (Figure 8). The ratio of plume heat flux to total CMB heat flux in numerical and laboratory models has also been analyzed by *Jellinek et al.* [2003] and *Gonnermann et al.* [2004]. Global plume anomalous mass and heat fluxes inferred from hot spot swells [*Davies*, 1988; *Sleep*, 1990] tend to imply even smaller ratios of plume to total mantle heat flux than in our model: compared to these estimates, the plumes in our model are still several times stronger.

[43] Future models should more systematically test the dependence of model results – whether upwellings are diffuse, sheetlike or plumelike, and where they form – only above the margins of domes or also above their interiors or even elsewhere – on various parameters, such as the amount of chemically distinct material (corresponding to the initial thickness of the layer) at the base of the mantle, the chemical density contrast, the thermal density contrast in

the TBL at the CMB, thermal diffusivity and hence the thickness of the TBL, the amount of viscosity drop in the TBL above the CMB, temperature dependence of viscosity, variations in viscosity due to different chemistry and the conditions for model initiation.

5. Conclusions

[44] Our model differs from previous models in that – for the first time – we report a realistic pattern of plumes forming mainly at margins of thermochemical domes, which form in response to subduction inferred from plate reconstructions over the past 300 Myr, similar to *McNamara and Zhong* [2005]. Subducted slabs sinking into the mantle cause large-scale mantle flow that forms a thermochemical layer at the base of the mantle into two domes resembling the African and Pacific LLSVPs in both size and shape. It also pushes a thermal boundary layer toward the domes. The boundary layer begins to rise along the steep margins of the domes, and rises to the surface predominantly in the form of plume-like upwellings. Key model ingredients needed to achieve that pattern are hence heat from the core, slabs sinking from the surface toward to base of the mantle and chemically distinct material (forming large "domes") at the base of the mantle. Plumes form at the locations (termed "Plume Generation Zones" by *Burke et al.* [2008]) where the core (presumed heat source), the LLSVPs and the rest of the mantle (containing the "slab graveyard") meet. Plate tectonics and mantle dynamics are coupled: Locations of subduction influence where plumes are formed on LLSVP margins, but where plumes rise may also decide where continents and plates break up. Future models will aim at achieving higher resolution, include lateral viscosity variations, and start with more realistic initial conditions. Outstanding open questions are how a realistic amount of entrainment of the chemical layer and long-term stability of LLSVPs can be achieved, while maintaining the formation of plumes on their margins.

Acknowledgments

[45] We thank Mike Gurnis and Paul Tackley for detailed and very helpful reviews, and Mark Jellinek for comments on an earlier version. This work greatly benefited from stays of both authors at the Centre for Advanced Study at the Norwegian Academy of Science and Letters 2010–2011. We would also like to thank Kevin Burke for motivating both of us to think about the problem addressed in this paper. Figures 1–5, 6 (top), 7, and 8 were prepared with the Generic Mapping Tools [*Wessel and Smith*, 1998].

References

Albers, M., and U. R. Christensen (1996), The excess temperature of plumes rising from the core-mantle boundary, *Geophys. Res. Lett.*, *23*, 3567–3570, doi:10.1029/96GL03311.

Anderson, D. L. (1981), Hotspots, basalts and the evolution of the mantle, *Science*, *213*, 82–89, doi:10.1126/science.213.4503.82.

Becker, T. W., and L. Boschi (2002), A comparison of tomographic and geodynamic mantle models, *Geochem. Geophys. Geosyst.*, *3*(1), 1003, doi:10.1029/2001GC000168.

Boschi, L., T. W. Becker, and B. Steinberger (2007), Mantle plumes: Dynamic models and seismic images, *Geochem. Geophys. Geosyst.*, *8*, Q10006, doi:10.1029/2007GC001733.

Bull, A. L., A. K. McNamara, and J. Ritsema (2009), Synthetic tomography of plume clusters and thermochemical piles, *Earth Planet. Sci. Lett.*, *278*, 152–162, doi:10.1016/j.epsl.2008.11.018.

Bunge, H.-P., and J. H. Davies (2001), Tomographic images of a mantle circulation model, *Geophys. Res. Lett.*, *28*, 77–80.

Burke, K., B. Steinberger, T. H. Torsvik, and M. A. Smethurst (2008), Plume generation zones at the margins of Large Low Shear Velocity Provinces on the core-mantle boundary, *Earth Planet. Sci. Lett.*, *265*, 49–60.

Davaille, A., and J. Vatteville (2005), On the transient nature of mantle plumes, *Geophys. Res. Lett.*, *32*, L14309, doi:10.1029/2005GL023029.

Davaille, A., E. Stutzmann, G. Silveira, J. Besse, and V. Courtillot (2005), Convective patterns under the Indo-Atlantic "box," *Earth Planet. Sci. Lett.*, *239*, 233–252, doi:10.1016/j.epsl.2005.07.024.

Davies, G. F. (1988), Ocean bathymetry and mantle convection: 1. Large-scale flow and hotspots, *J. Geophys. Res.*, *93*, 10,467–10,480, doi:10.1029/JB093iB09p10467.

de Koker, N. (2010), Thermal conductivity of MgO periclase at high pressure: Implications for the D″ region, *Earth Planet. Sci. Lett.*, *292*, 392–398, doi:10.1016/j.epsl.2010.02.011.

Dziewonski, A. M. (1984), Mapping the lower mantle: Determination of lateral heterogeneity in P velocity up to degree and order 6, *J. Geophys. Res.*, *89*, 5929–5952, doi:10.1029/JB089iB07p05929.

Dziewonski, A. M., and D. L. Anderson (1981), Preliminary reference Earth model, *Phys. Earth Planet. Inter.*, *25*, 297–356, doi:10.1016/0031-9201(81)90046-7.

Dziewonski, A. M., B. A. Romanowicz, and V. Lekic (2010), Mantle anchor structure: An argument for bottom up tectonics, *Earth Planet. Sci. Lett.*, *299*, 69–79, doi:10.1016/j.epsl.2010.08.013.

Garnero, E. J., and A. K. McNamara (2008), Structure and dynamics of Earth's lower mantle, *Science*, *320*, 626–628, doi:10.1126/science.1148028.

Garnero, E. J., T. Lay, and A. McNamara (2007), Implications of lower-mantle structural heterogeneity for existence and nature of whole-mantle plumes, *Spec. Pap. Geol. Soc. Am.*, *430*, 79–88.

Goncharov, A. F., P. Beck, V. V. Struzhkin, B. D. Haugen, and S. D. Jacobsen (2009), Thermal conductivity of lower-mantle minerals, *Phys. Earth Planet. Inter.*, *174*, 24–32, doi:10.1016/j.pepi.2008.07.033.

Goncharov, A. F., V. V. Struzhkin, J. A. Montoya, S. Kharlamova, R. Kundargi, J. Siebert, J. Badro, D. Antonangeli, F. J. Ryerson, and W. Mao (2010), Effect of composition, structure, and spin

state on the thermal conductivity of the Earth's lower mantle, *Phys. Earth Planet. Inter.*, *180*, 148–153, doi:10.1016/j.pepi.2010.02.002.

Gonnermann, H. M., A. M. Jellinek, M. A. Richards, and M. Manga (2004), Modulation of mantle plumes and heat flow at the core mantle boundary by plate-scale flow: Results from laboratory experiments, *Earth Planet. Sci. Lett.*, *226*, 53–67, doi:10.1016/j.epsl.2004.07.021.

Grand, S. P., R. D. Van der Hilst, and S. Widiyantoro (1997), Global seismic tomography: A snapshot of convection in the Earth, *GSA Today*, *7*, 1–7.

Gurnis, M. (1986), The effects of chemical density differences on convective mixing in the Earth's mantle, *J. Geophys. Res.*, *91*, 11,407–11,419, doi:10.1029/JB091iB11p11407.

Gurnis, M., S. Zahirovic, M. Turner, L. DiCaprio, S. Spasojevic, R. D. Müller, J. Boyden, M. Seton, V. C. Manea, and D. J. Bower (2012), Plate reconstructions with continuously closing plates, *Comput. Geosci.*, *38*, 35–42.

Hager, B. H., and R. J. O'Connell (1979), Kinematic models of large-scale flow in the Earth's mantle, *J. Geophys. Res.*, *84*, 1031–1048, doi:10.1029/JB084iB03p01031.

Hager, B. H., and R. J. O'Connell (1981), A simple global model of plate dynamics and mantle convection, *J. Geophys. Res.*, *86*, 4843–4867, doi:10.1029/JB086iB06p04843.

Hernlund, J. W., and C. Houser (2008), On the statistical distribution of seismic velocities in Earth's deep mantle, *Earth Planet. Sci. Lett.*, *265*, 423–437, doi:10.1016/j.epsl.2007.10.042.

Hofmeister, A. M. (2008), Inference of high thermal transport in the lower mantle from laser-flash experiments and the damped harmonic oscillator model, *Phys. Earth Planet. Inter.*, *170*, 201–206, doi:10.1016/j.pepi.2008.06.034.

Ishii, M., and J. Tromp (2004), Constraining large-scale mantle heterogeneity using mantle and inner-core sensitive normal modes, *Phys. Earth Planet. Inter.*, *146*, 113–124, doi:10.1016/j.pepi.2003.06.012.

Jellinek, M., and M. Manga (2002), The influence of a chemical boundary layer on the fixity, spacing and lifetime of mantle plumes, *Nature*, *418*, 760–763, doi:10.1038/nature00979..

Jellinek, M., and M. Manga (2004), Links between long-lived hotspots, mantle plumes, D″ and plate tectonics, *Rev. Geophys.*, *42*, RG3002, doi:10.1029/2003RG000144.

Jellinek, M., H. M. Gonnermann, and M. A. Richards (2003), Plume capture by divergent plate motions: Implications for the distribution of hotspots, geochemistry of mid-ocean ridge basalts, and estimates of the heat flux at the core-mantle boundary, *Earth Planet. Sci. Lett.*, *205*, 361–378, doi:10.1016/S0012-821X(02)01070-1.

Korenaga, J. (2005), Firm mantle plumes and the nature of the core-mantle boundary region, *Earth Planet. Sci. Lett.*, *232*, 29–37, doi:10.1016/j.epsl.2005.01.016.

Lassak, T. M., A. K. McNamara, E. J. Garnero, and S. Zhong (2010), Core-mantle boundary topography as a possible constraint on lower mantle chemistry and dynamics, *Earth Planet. Sci. Lett.*, *289*, 232–241.

Lay, T., E. J. Garnero, and Q. Williams (2004), Partial melting in a thermo-chemical boundary layer at the base of the mantle, *Phys. Earth Planet. Inter.*, *146*, 441–467.

Lay, T., J. Hernlund, and B. A. Buffett (2008), Core-mantle boundary heat flow, *Nat. Geosci.*, *1*, 25–32, doi:10.1038/ngeo.2007.44.

Loper, D. E., and F. D. Stacey (1983), The dynamical and thermal structure of deep mantle plumes, *Phys. Earth Planet. Inter.*, *33*, 304–317, doi:10.1016/0031-9201(83)90047-X.

Masters, G., G. Laske, H. Bolton, and A. Dziewonski (2000), The relative behavior of shear velocity, bulk sound speed, and compressional velocity in the mantle: Implications for chemical and thermal structure, in *Earth's Deep Interior: Mineral Physics and Tomography From the Atomic to Global Scale*, *Geophys. Monogr. Ser.*, vol. 117, edited by S.-I. Karato et al., pp. 63–87, AGU, Washington, D. C., doi:10.1029/GM117p0063.

McNamara, A., and S. Zhong (2005), Thermochemical structures beneath Africa and the Pacific Ocean, *Nature*, *437*, 1136–1139, doi:10.1038/nature04066.

Monnereau, M., and S. Quere (2001), Spherical shell models of mantle convection with tectonic plates, *Earth Planet. Sci. Lett.*, *184*, 575–587.

Morgan, W. J. (1971), Convection plumes in the lower mantle, *Nature*, *230*, 42–43.

Morgan, W. J. (1972), Deep mantle convection plumes and plate motions, *Am. Assoc. Pet. Geol. Bull.*, *56*, 203–213.

Nakagawa, T., and P. Tackley (2005), Deep mantle heat flow and thermal evolution of the Earth's core in thermochemical multiphase models of mantle convection, *Geochem. Geophys. Geosyst.*, *6*, Q08003, doi:10.1029/2005GC000967.

Nataf, H.-C. (1991), Mantle convection, plates and hotspots, *Tectonophysics*, *187*, 361–371, doi:10.1016/0040-1951(91)90475-8.

Ni, S., E. Tan, M. Gurnis, and D. Helmberger (2002), Sharp sides to the African superplume, *Science*, *296*, 1850–1852, doi:10.1126/science.1070698.

Olson, P., and C. Kincaid (1991), Experiments on the interaction of thermal convection and compositional layering at the base of the mantle, *J. Geophys. Res.*, *96*, 4347–4354.

Panasyuk, S. V., B. H. Hager, and A. M. Forte (1996), Understanding the effect of mantle compressibility on geoid kernels, *Geophys. J. Int.*, *124*, 121–133.

Press, W. H., B. P. Flannery, S. A. Teukolsky, and W. T. Vetterling (1986), *Numerical Recipes: The Art of Scientific Computing*, Cambridge Univ. Press, Cambridge, U. K.

Richards, M. A., R. A. Duncan, and V. E. Courtillot (1989), Flood basalts and hotspot tracks: Plume heads and tails, *Science*, *246*, 103–107, doi:10.1126/science.246.4926.103.

Robin, C., A. M. Jellinek, V. Tahyalan, and A. Lenardic (2007), Transient mantle convection on Venus: The paradoxical coexistence of highlands and coronae in the BAT region, *Earth Planet. Sci. Lett.*, *256*, 100–119, doi:10.1016/j.epsl.2007.01.016.

Schubert, G., D. L. Turcotte, and P. Olson (2001), *Mantle Convection in the Earth and Planets*, Cambridge Univ. Press, New York, doi:10.1017/CBO9780511612879.

Sleep, N. H. (1990), Hotspots and mantle plumes: Some phenomenology, *J. Geophys. Res.*, *95*, 6715–6736, doi:10.1029/JB095iB05p06715.

Sleep, N. H., M. A. Richards, and B. H. Hager (1988), Onset of mantle plumes in the presence of preexisting convection, *J. Geophys. Res.*, *93*, 7672–7689, doi:10.1029/JB093iB07p07672.

Stackhouse, S., L. Stixrude, and B. B. Karki (2010), Thermal conductivity of periclase (MgO) from first principles, *Phys. Rev. Lett.*, *104*, 208501, doi:10.1103/PhysRevLett.104.208501.

Steinberger, B. (2000), Plumes in a convecting mantle: Models and observations for individual hotspots, *J. Geophys. Res.*, *105*, 11,127–11,152, doi:10.1029/1999JB900398.

Steinberger, B., and M. Antretter (2006), Conduit diameter and buoyant rising speed of mantle plumes: Implications for the motion of hotspots and shape of plume conduits, *Geochem. Geophys. Geosyst.*, *7*, Q11018, doi:10.1029/2006GC001409.

Steinberger, B., and A. Calderwood (2006), Models of large-scale viscous flow in the Earth's mantle with constraints from mineral physics and surface observations, *Geophys. J. Int.*, *167*, 1461–1481, doi:10.1111/j.1365-246X.2006.03131.x.

Steinberger, B., and R. J. O'Connell (1998), Advection of plumes in mantle flow: Implications on hotspot motion, mantle viscosity and plume distribution, *Geophys. J. Int.*, *132*, 412–434, doi:10.1046/j.1365-246x.1998.00447.x.

Steinberger, B., and T. H. Torsvik (2008), Absolute plate motions and true polar wander in the absence of hotspot tracks, *Nature*, *452*, 620–623, doi:10.1038/nature06824.

Steinberger, B., and T. H. Torsvik (2010), Explanation for the present and past locations of the poles, *Geochem. Geophys. Geosyst.*, *11*, Q06W06, doi:10.1029/2009GC002889.

Tackley, P. J. (1998), Three-dimensional simulations of mantle convection with a thermochemical CMB boundary layer: D″?, in *The Core-Mantle Boundary Region*, *Geodyn. Ser.*, vol. 28, edited by M. Gurnis et al., pp. 231–253, AGU, Washington, D. C., doi:10.1029/GD028p0231.

Tackley, P. J. (2011), Living dead slabs in 3-D: The dynamics of compositionally stratified slabs entering a "slab graveyard" above the core-mantle boundary, *Phys. Earth Planet. Inter.*, *188*, 150–162.

Tan, E., and M. Gurnis (2005), Metastable superplumes and mantle compressibility, *Geophys. Res. Lett.*, *32*, L20307, doi:10.1029/2005GL024190.

Tan, E., M. Gurnis, and L. Han (2002), Slabs in the lower mantle and their modulation of plume formation, *Geochem. Geophys. Geosyst.*, *3*(11), 1067, doi:10.1029/2001GC000238.

Tan, E., E. Choi, P. Thoutireddy, M. Gurnis, and M. Aivazis (2006), GeoFramework: Coupling multiple models of mantle convection within a computational framework, *Geochem. Geophys. Geosyst.*, *7*, Q06001, doi:10.1029/2005GC001155.

Tan, E., W. Leng, S. Zhong, and M. Gurnis (2011), On the location of plumes and mobility of thermo-chemical structures with high bulk modulus in the 3-D compressible mantle, *Geochem. Geophys. Geosyst.*, *12*, Q07005, doi:10.1029/2011GC003665.

Thorne, M. S., E. J. Garnero, and S. Grand (2004), Geographic correlation between hot spots and deep mantle lateral shear-wave velocity gradients, *Phys. Earth Planet. Inter.*, *146*, 47–63, doi:10.1016/j.pepi.2003.09.026.

Torsvik, T. H., M. A. Smethurst, K. Burke, and B. Steinberger (2006), Large igneous provinces generated from the margins of the large low-velocity provinces in the deep mantle, *Geophys. J. Int.*, *167*, 1447–1460, doi:10.1111/j.1365-246X.2006.03158.x.

Torsvik, T. H., R. D. Müller, R. Van der Voo, B. Steinberger, and C. Gaina (2008), Global plate motion frames: Toward a unified model, *Rev. Geophys.*, *46*, RG3004, doi:10.1029/2007RG000227.

Torsvik, T. H., K. Burke, B. Steinberger, S. J. Webb, and L. D. Ashwal (2010), Diamonds sampled by plumes from the core-mantle boundary, *Nature*, *466*, 352–355, doi:10.1038/nature09216.

Trampert, J., F. Deschamps, J. S. Resovsky, and D. Yuen (2004), Probabilistic tomography maps significant chemical heterogeneities in the lower mantle, *Science*, *306*, 853–856, doi:10.1126/science.1101996.

van der Meer, D., W. Spakman, D. J. J. van Hinsbergen, M. L. Amaru, and T. H. Torsvik (2010), Towards absolute plate motions constrained by lower-mantle slab remnants, *Nat. Geosci.*, *3*, 36–40, doi:10.1038/ngeo708.

Wang, Y., and L. Wen (2004), Mapping the geometry distribution of a very low velocity province at the base of the Earth's mantle, *J. Geophys. Res.*, *109*, B10305, doi:10.1029/2003JB002674.

Wessel, P., and W. H. F. Smith (1998), New, improved version of the Generic Mapping Tools released, *Eos Trans. AGU*, *79*, 579, doi:10.1029/98EO00426.

Wilson, J. T. (1963), A possible origin of the Hawaiian Islands, *Can. J. Phys.*, *41*, 863–870, doi:10.1139/p63-094.

Zhang, N., S. Zhong, and A. K. McNamara (2009), Supercontinent formation from stochastic collision and mantle convection models, *Gondwana Res.*, *15*, 267–275, doi:10.1016/j.gr.2008.10.002.

Zhang, N., S. Zhong, W. Leng, and Z.-X. Li (2010), A model for the evolution of the Earth's mantle structure since the Early Paleozoic, *J. Geophys. Res.*, *115*, B06401, doi:10.1029/2009JB006896.